Band structure of indium phosphide from near-band-gap photoemission

J. Peretti, H.-J. Drouhin, and D. Paget
Laboratoire de Physique de la Matière Condensée, Ecole Polytechnique, F-91128 Palaiseau, France

A. Mircéa
Centre National d'Etudes des Télécommunications, 196 Avenue Henri-Ravera, F-92220 Bagneux, France
(Received 11 December 1990)

Energy analysis of the electrons photoemitted from *p*-type doped (100) InP crystals is performed with 20-meV resolution, at 120 K. The samples are activated to low electron affinity. Laser excitation in the photon energy range $1.96 \leq h\nu \leq 3.53$ eV is used. The locations of the subsidiary minima L_6 and X_6 of the first conduction band and X_{7c} of the second one are unambiguously measured (respectively, 0.67, 0.90, and 1.18 eV above the bottom of the conduction band). The energy dispersion of the three upper valence bands and of the first conduction band is probed over a large portion of the Brillouin zone. These experimental results are accurately described in the framework of the $\mathbf{k}\cdot\mathbf{p}$ Kane model and the value of the spin-orbit-split-band mass $m_7=(0.19\pm0.01)m_0$ (where m_0 is the free-electron mass) is directly obtained.

I. INTRODUCTION

Indium phosphide is a semiconductor of growing technological importance, especially for the design of transferred-electron devices. However, its band structure is not as accurately known as the gallium arsenide one. In particular, the locations of the subsidiary minima L_6 and X_6 of the first conduction band remain controversial. In the literature, the values, referred to Γ_{6c}, the bottom of the first conduction band, range from 0.39 to 0.86 eV for L_6 and from 0.66 to 1.40 eV for X_6. In the present work, we use high-resolution energy analysis of near-band-gap photoemission to investigate the InP band structure. This technique, developed by Drouhin, Hermann, and Lampel for the study of GaAs, and the data analysis procedure are described in detail in Ref. 1; in the following, we only briefly recall the main points. That way, we directly measure the energy positions of the side minima L_6, X_6 of the first conduction band and X_{7c} of the second one and we probe the energy dispersion of the upper valence bands (the heavy-hole, light-hole, and spin-orbit-split bands, hereafter, respectively, referred to as Γ_{8h}, Γ_{8l}, and Γ_7) and of the first conduction band (the Γ_6 band) over a large portion of the first Brillouin zone. Starting from the Kane $\mathbf{k}\cdot\mathbf{p}$ perturbation model,[2] we use simple analytical approximations of the band dispersion[3] to check the sensitivity of our experimental results to various parameters. We prove that such an experiment is an original technique for the measurement of effective masses.

II. EXPERIMENT

Two (100) InP samples are used in the present study: a *p*-type (2×10^{18} cm^{-3}) metal-organic chemical vapor deposition (MOCVD) -grown layer covered by an As-passivating cap (sample 1) and a *p*-type doped (5×10^{18} cm^{-3}) commercial crystal (sample 2). Sample 1 did not undergo any chemical etching while sample 2 was chemically etched in a 0.3% bromine-methanol solution and decanted with isopropanol. Then, they were introduced into an ultrahigh-vacuum chamber (pressure in the low 10^{-11} Torr range) through a glove box under nitrogen circulation and an introduction lock. The whole introduction procedure takes about 1 h. Subsequently, the crystal surface is heat cleaned during a few hours at 620 K. At this temperature, the InP stoichiometry is preserved and, in the case of sample 1, the As-top layer is desorbed. The crystal-surface work function is finally lowered by the standard activation procedure of Cs and O_2 deposition.[1]

The sample is irradiated through two different light sources: a 1.96-eV He-Ne laser and a krypton-ion laser (both focused on a radius $\sim$0.3 mm). At these photon energies, the optical-absorption length is of the order of a few thousand angstroms so that a significant part of the light absorption takes place in the bulk solid (the band-bending region is about 300 Å thick for this doping level). The photoelectrons are energy-analyzed with 20-meV energy resolution using a homemade electron spectrometer.[4] The measurements we report here are all performed at 120 K, the sample holder being cooled down by liquid-nitrogen circulation.

For reasons which remain not completely understood, the energy distribution curves (EDC's) exhibit features which are much more difficult to resolve than in the case of GaAs. We observed that the value of the total emitted current has to be maintained below 300 nA to obtain well-resolved spectra (compared to a few μA in the same experimental conditions with GaAs). Then the energy-analyzed current is of the order of 0.3 nA. Therefore, to achieve reliable measurements in the EDC high-energy part, we use an accumulation procedure such that recording a photoemission spectrum takes about half an hour.

It also appeared that the surface preparation of InP photocathodes plays a crucial role with respect to their photoemission properties. Consequently, the present study of the InP band structure requires much more technological work than that of the GaAs one. Extreme care was brought to sample cleaning and to vacuum quality. Related work of our group is devoted to the photoemission properties of Ag/InP Schottky diodes[5,6] and we observed that a thin (about 100 Å) Ag film deposited on the semiconductor surface makes the structures in the photoemission spectra more apparent, while never altering their position. In this case, an electrically continuous Ag layer is evaporated at a rate of about 1 Å/s, at room temperature, while the pressure is kept below 2×10^{-10} Torr. The Ag surface is then activated to low electron affinity.

III. EXPERIMENTAL RESULTS

Figure 1 shows two EDC's and their derivatives recorded under excitation at $h\nu=1.96$ eV. These EDC's are relatively similar to the corresponding GaAs curves, which are studied in Ref. 1. The intense low-energy peak originates from electrons which, in the bulk crystal, were thermalized at the bottom of the first conduction band. Information on the band dispersion is contained in the high-energy part of the spectrum and is revealed in the derivatives where features are clearly observed. The comparison between curves *a* (sample 1 coated with a Ag film) and *b* (sample 2 without Ag film) shows that the position of the high-energy features (which are more pronounced on curve *a*) is completely identical, with the exception of an additional structure at the high-energy edge of curve *a*. This latter is due to electrons excited in the Ag layer. Its high-energy threshold corresponds to electrons photoemitted from the Fermi level (energy E_F) and provides an absolute energy reference by defining the energy $E_F+h\nu$. Because, after activation to low-electron affinity and cooling down the crystal temperature to 120 K, the metallized sample has a lower work function than the unmetallized sample, a low-energy structure corresponding to electrons excited from the Γ_7 band is only observed in curve *a*.

Figure 2 shows EDC derivatives from the metallized samples recorded for different excitation energies. This

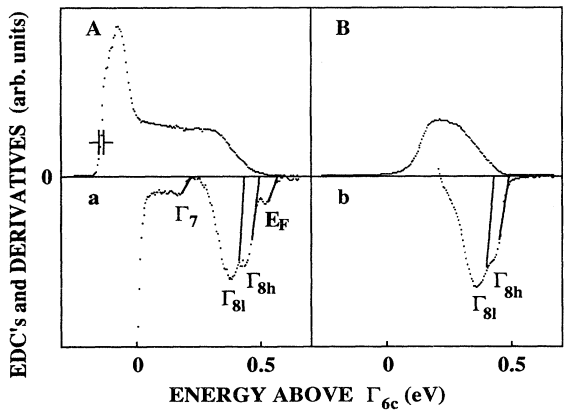

FIG. 1. EDC's (curves *A* and *B*) and their derivatives (curves *a* and *b*) of electrons emitted from a InP photocathode at 120 K, for 1.96-eV excitation energy. The energy of the photoemitted electrons is referred to the bulk position of Γ_{6c}, the minimum of the first conduction band. Curves *A* and *a* (*B* and *b*) are obtained from sample 1 (sample 2) with (without) a 100-Å-thick Ag top layer. The extrapolation procedure, shown on the derivatives, has been described in Ref. 1 and is used here to determine the promotion energies of electrons excited from the upper valence bands and from the Ag Fermi level (the corresponding structures are labeled Γ_{8h}, Γ_{8l}, Γ_7, and E_F). The uncertainties on the determination of the final-state energies introduced through this procedure are of the order of the experimental resolution represented by —||—.

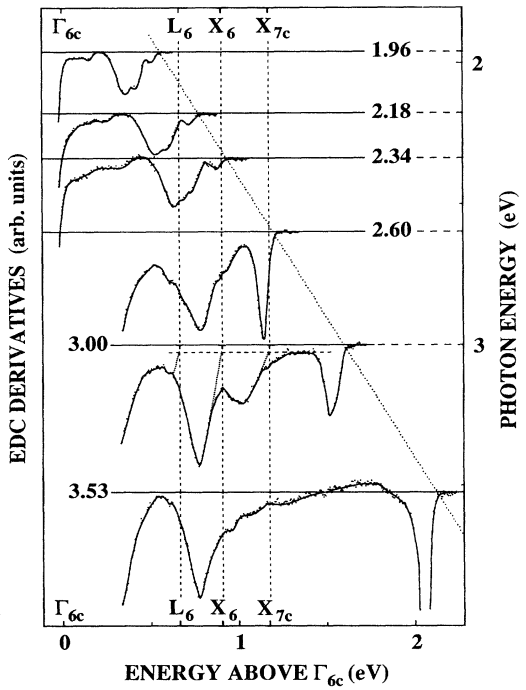

FIG. 2. Derivatives of the EDC's at 120 K, for different excitation energies. The energy of the photoemitted electrons is referred to the bulk position of Γ_{6c}. For clarity, the low-energy parts of the curves have been omitted. The curves are shifted along the vertical axis so that their base line corresponds to the excitation energy. The 1.96-, 2.18-, and 2.34-eV spectra are obtained on sample 1 (identical results but with not so well-resolved structures were also obtained with sample 2). The 2.60-, 3.00-, and 3.53-eV spectra are obtained on sample 2 (its larger work function allows a more intense optical excitation for a given emitted current, under stable conditions, and thus it reveals the higher-energy structures more clearly than sample 1). A 100-Å-thick Ag layer is evaporated on both samples. The dotted line of slope 1 corresponds to the creation energy of electrons excited, in the Ag layer, from the Fermi level. The bulk positions of the L_6, X_6, and X_{7c} minima are indicated by vertical dashed lines. They are also marked on the energy axis as well as the bulk position of the Γ_{6c} minimum. The extrapolation procedure is shown on the spectrum recorded with $h\nu=3$ eV, for the determination of the side-valley locations.

shows two types of structures (some of them are small but can always be resolved). The structures occurring at fixed energies, whatever $h\nu$ when observed, reveal electrons accumulated in the conduction minima. The structures whose position depends on $h\nu$ correspond to final states of optical transitions from the valence to the conduction states. Because, at low temperature, energy gain by phonon absorption is negligible, the high-energy threshold of the structures is, depending on their type, characteristic of the conduction minima or of the final-state location.[1]

IV. ANALYSIS

For analysis, we draw the photoemission structure diagram, i.e., we plot the experimental location of the high-energy threshold of each structure as a function of $h\nu$ (Fig. 3). This procedure clearly selects energies referring to phenomena occurring in the bulk semiconductor because, when they occur in the band-bending region, their contribution is down shifted in energy.

A. $h\nu$-independent structures: conduction side-valley location

The positions of the $h\nu$-independent structures correspond to the locations of the conduction minima. Assuming the usual Γ_{6c}, L_6, X_6 ordering,[7] the Γ_{6c}-L_6, Γ_{6c}-X_6, and Γ_{6c}-X_{7c} spacings are, respectively, equal to 0.67, 0.90, and 1.18 eV. The uncertainties on these measurements are of the order of the energy resolution for X_6 and X_{7c} and probably twice as large for L_6 because the high-energy edge of the associated structure is not so well defined. These values are compared with previous results in Table I. The data are clearly distributed in two groups. Those obtained from optical measurements are consistent with the present determination (except for the one given in Footnote o of Table I). Those deduced from transport properties, a less direct approach, correspond to lower values. An exception is our field-assisted photoemission experiment,[6] which involves both transport properties and optical techniques and provides data in good agreement with the present photoemission experiment. The location of the X_{7c} minima had in fact never been really measured previously. Such data is important as an input parameter in band-structure models: that is all the more interesting that our value notably differs from the pseudopotential calculation of Ref. a in Table I.

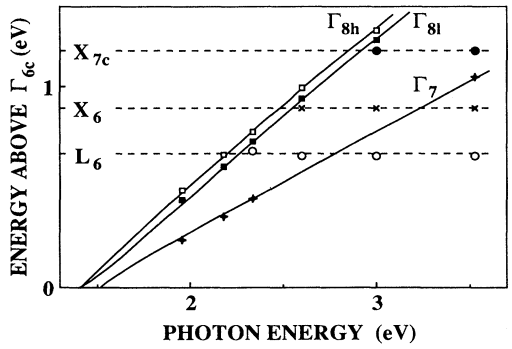

FIG. 3. InP structure diagram at 120 K, i.e., plot of the high-energy threshold of the structures (referred to the bulk position of Γ_{6c}, the minimum of the conduction band) as a function of the photon energy. The symbols correspond to the experimental data. The □, ■, and + refer, respectively, to the $\Gamma_{8h}\rightarrow\Gamma_6$, $\Gamma_{8l}\rightarrow\Gamma_6$, and $\Gamma_7\rightarrow\Gamma_6$ transitions; the ●, ×, and ○ correspond, respectively, to electrons accumulated into the L_6, X_6, and X_{7c} subsidiary minima. The full lines are calculated in the framework of the Kane model for transitions from the three upper valence bands Γ_{8h}, Γ_{8l}, and Γ_7. The experimental bulk locations of the L_6, X_6, and X_{7c} subsidiary minima are indicated by horizontal dashed lines.

B. $h\nu$-dependent structures: band dispersion, effective-mass measurement

The analysis of the $h\nu$-dependent structures involves both valence- and conduction-state dispersion and requires a band-structure model. Because in the photon energy range that we use the optical transitions occur at notable values of the wave-vector modulus k, this band model has to take into account band nonparabolicity. Within the limits of our experimental resolution, the Kane perturbation model[2] is well suited.[1] We perform the *numerical* calculation of the band dispersion along the [100] direction, i.e., the normal to the crystal surface, neglecting the band-anisotropy effects which remain well within our error bars (of the order of our energy resolution) in the whole part of the Brillouin zone that we experimentally probe. The model makes use of the values of the band-gap energy $E_G=1.405$ eV (Ref. 8) (± 0.005 eV, this error bar being essentially related to the uncertainty on our measurement of the sample temperature), of the spin-orbit-splitting energy $\Delta=0.108\pm0.003$ eV,[9] of the momentum matrix element between valence and conduction states which is characterized by $P^2=20.7\pm1.5$ eV (Ref. 10) [this value is related to the Kane parameter $\mathcal{P}^2$ by $P^2=(2m_0/\hbar^2)\mathcal{P}^2$, where m_0 is the free-electron mass]. It also involves the Kane parameter combinations $\mathcal{A}+\mathcal{B}$, $\mathcal{C}+\mathcal{D}$, and $\mathcal{F}$, which define the remote-band interactions: they will be deduced from the experimental values of the conduction mass and two of the three valence masses. In the following, we consider the influence of the parameters which can be slightly adjusted on the promotion energies of electrons excited into the conduction band from the different valence bands, i.e. on the fit of the photoemission structure diagram. In Sec. IV B 1 we first give a very simplified band model, which is intended as a guide, and justify that the light-hole mass value does not enter into our calculation. Then, in Sec. IV B 2 we demonstrate that the uncertainty on P^2 has a negligible effect on the numerical results. Finally, in Sec. IV B 3 we analyze the sensitivity of our calculation to the effective-mass values and show that our measurements provide a direct and accurate estimation of the spin-orbit-split band mass. The main steps of this *analytical* treatment are given in the Appendix.

TABLE I. Experimental determinations of the energy positions of InP subsidiary minima, L_6 and X_6 in the first conduction band and X_{7c} in the second one. The values are referred to Γ_{6c}, the minimum of the conduction band at the zone center. The data presented in this table were obtained at 300 K except where noted. For comparison, the theoretical results of the nonlocal pseudopotential calculation of Chelikowsky and Cohen are also reported here.

Authors	L_6	X_6	X_{7c}	Method or technique
Chelikowsky and Cohen[a]	0.69	0.94	1.47	Nonlocal pseudopotential calculation
Pitt[b]	0.40	0.70		High-pressure Hall measurements
Pitt and co-workers[c]	0.50	0.85		Same technique
Maloney *et al.*[d]	0.53	0.73	1.03	Monte Carlo calculations on Ag/InP Schottky diodes photoemission properties
Adachi[e]	0.70	0.86		Fit of the dielectric function spectra
Hakki, Jayaraman, and Kim[f]		0.66		Extrapolation of high-pressure *p-n* junction data on $In_{1-x}Al_xP$
Rodot *et al.*[g]		0.81		Extrapolation of optical-absorption data on $In_{1-x}Al_xP$
Hilsum and Porteous[h]		0.80		Extrapolation of luminescence measurements on $In_{1-x}Ga_xP$
Mabbitt[i]		0.76		Extrapolation of cathodoluminescence measurements on $In_{1-x}Ga_xP$
Mabbitt[i]		0.87		Same technique (77 K)
Onton, Lorenz, and Reuter[j]		0.90		Same technique
Onton and Chicotka[k]		0.90		Same technique on $In_{1-x}Al_xP$
Onton and co-workers[l]		0.96		Infrared absorption (8 K)
Dumke, Lorenz, and Pettit[m]		0.90		Same technique (77 K)
Drube, Straub, and Himpsel[n]		1.4	1.4	Inverse photoemission
Alekseev *et al.*[o]	0.86			Hot-photoluminescence spectroscopy
Majerfeld and co-workers[p]	0.39			Deduced from deep-level-trap activation energy and energy position measurements
James *et al.*[q]	0.61			Near-band-gap photoemission
Peretti, Drouhin, and Paget[r]	0.64	0.87	1.15	Field-assisted photoemission (120 K)
This work	0.67	0.90	1.18	Near-band-gap photoemission (120 K)

[a]J. M. Chelikowsky and M. L. Cohen, Phys. Rev. B **14**, 556 (1976).
[b]Reference 7.
[c]G. D. Pitt, K. R. Vyas, and A. W. Mabbitt, Solid State Commun. **14**, 621 (1974); G. D. Pitt, J. Phys. C **6**, 1586 (1973).
[d]T. J. Maloney, M. G. Burt, J. S. Escher, P. E. Gregory, S. B. Hyder, and G. A. Antypas, J. Appl. Phys. **51**, 2879 (1980). The position of the X_{7c} valley has been taken from Fig. 1.
[e]S. Adachi, Phys. Rev. B **35**, 7454 (1987).
[f]B. W. Hakki, A. Jayaraman, and C. K. Kim, J. Appl. Phys. **41**, 5291 (1970).
[g]H. Rodot, J. Horak, G. Rouy, and J. Bourneix, C. R. Acad. Sci. B **269**, 381 (1969).
[h]C. Hilsum and P. Porteous, *Proceedings of the Ninth International Conference on the Physics of Semiconductors, Moscow, 1968* (Nauka, Moscow, 1968), p. 1214.
[i]A. W. Mabbitt, Solid State Commun. **9**, 245 (1971).
[j]A. Onton, M. R. Lorenz, and W. Reuter, J. Appl. Phys. **42**, 3420 (1971).
[k]A. Onton and R. J. Chicotka, J. Appl. Phys. **41**, 4205 (1970).
[l]A. Onton, Y. Yacobi, and R. J. Chicotka, Phys. Rev. Lett. **28**, 966 (1972); A. Onton, R. J. Chicotka, and Y. Yacobi, *Proceedings of the Eleventh International Conference on the Physics of Semiconductors, Warsaw, 1972,* (PWN Polish Scientific Publishers, Warsaw, 1972), p. 1023.
[m]W. P. Dumke, M. R. Lorenz, and G. D. Pettit, Phys. Rev. B **1**, 4668 (1970).
[n]W. Drube, D. Straub, and F. J. Himpsel, Phys. Rev. B **35**, 5563 (1987). In this experiment, the positions of the X_6 and X_{7c} side valleys are not resolved.
[o]M. A. Alekseev, I. Ya. Karlik, D. N. Mirlin, V. F. Sapega, and A. A. Sirenko, *Proceedings of the Nineteenth International Conference on the Physics of Semiconductors, Warsaw, 1988,* edited by W. Zawadzki (Institute of Physics Polish Academy of Sciences, Warsaw, 1988), p. 1423.
[p]A. Majerfeld, O. Wada, and A. N. M. M. Choudhury, Appl. Phys. Lett. **33**, 957 (1978); O. Wada, A. Majerfeld, and A. N. M. M. Choudhury, J. Appl. Phys. **51**, 423 (1980).
[q]Reference 14.
[r]Reference 6.

1. Physical insight into the band-structure model

A striking feature of the model is that, in the absence of the remote-band interaction and *at the limit of large wave vector,* the bands become linear in k (neglecting $\hbar^2k^2/2m_0$ terms):

$$\varepsilon_6 \approx k\mathcal{P}+(3E_G-\Delta)/6 , \quad (1)$$

$$\varepsilon_7 \approx -k\mathcal{P}+(3E_G-\Delta)/6 , \quad (2)$$

$$\varepsilon_{8h} \approx 0 , \quad (3)$$

$$\varepsilon_{8l} \approx -2\Delta/3 , \quad (4)$$

where k is the wave vector and ε_6, ε_7, ε_{8h}, and ε_{8l}, respectively, refer to the energies of electrons in the Γ_6, Γ_{8h}, Γ_{8l}, and Γ_7 bands, with the origin at the top of the heavy-hole band.[11] In particular the Γ_{8l} band becomes parallel to the Γ_{8h} band and distant by $2\Delta/3$. This result still holds when one adds the remote-band interaction which determines the heavy-hole effective mass. It is in fact nearly the case in the domain investigated in our photon energy range, as evidenced by the parallel lines corresponding to the $\Gamma_{8h}\rightarrow\Gamma_6$ and $\Gamma_{8l}\rightarrow\Gamma_6$ optical transitions in the structure diagram (Fig. 3); from their energy separation, a more precise analysis (see Sec. 2 C of the Appendix) allows a direct estimation of the spin-orbit energy, $\Delta=0.114\pm0.025$ eV. Consequently, our experiment is not sensitive to the shape of the Γ_{8l} band near the zone center and we shall not put in the numerical calculation the light-hole mass value m_{8l} which is known only within 10%.[12] We rather make use of the heavy-hole-mass value $m_{8h}=(0.56\pm0.02)m_0$ in the [100] direction[12] and the conduction mass $m_6=(0.0765\pm0.0005)m_0$,[13] which have both been accurately measured in cyclotron resonance experiments, and of the spin-orbit-split-band mass value m_7 that we treat here as an *adjustable* parameter. This mass, which has so far not been precisely measured, is determined from our experimental data (see Sec. IV B 3).

2. Influence of the momentum matrix element

We now consider the influence of P^2 on the band structure, at large k. For instance, the variation of ε_6 *at fixed* k when changing P^2 by δP^2 is [using Eq. (1)] of the order of $(k\mathcal{P}/2)(\delta P^2/P^2)$, which can be larger than our experimental energy resolution. Nevertheless, the promotion energies into the conduction band associated with the transitions from the different valence bands *at a given* $h\nu$ remain almost unaffected. This would be obvious in the simple model of Sec. IV B 1 because the Γ_{8h} and Γ_{8l} bands are flat bands and the Γ_7 and Γ_6 bands are mirror bands.

In the framework of the Kane model, the calculation indeed yields a change of the promotion energy into the Γ_6 band from the Γ_{8l} or Γ_{8h} bands (see Sec. 2 a of the Appendix) which is only a fraction of the quantity $-k\mathcal{P}(k\mathcal{P}/P^2)(m_0/m_{8h})(\delta P^2/P^2)$, i.e., $\varepsilon_{8h}(\delta P^2/P^2)$. In the case of the promotion energy $\varepsilon_{7\text{-}6}$ from the Γ_7 band (see Sec. 3 a of the Appendix), the energy change is of the order of $-(k\mathcal{P}/3)(\delta P^2/P^2)(k\mathcal{P}/E_G)(\Delta/E_G)$.

To estimate these variations at a given value of $h\nu$, $(k\mathcal{P})^2$ has to be taken as nearly equal to $h\nu(h\nu-E_G)$ in the first case and to $[(h\nu)^2-E_G^2]/4$ in the second case [see Eqs. (A4) and (A7)]. Thus, in both cases, the promotion energy change remains much smaller than our energy resolution, in the meV range for P^2 varying within its error bar. Therefore, the fit of the $h\nu$-dependent lines in the structure diagram is nearly insensitive to the P^2 parameter.

3. Sensitivity to effective masses

In the same way, we consider the influence of the remote-band interaction on the promotion energies into the conduction band for optical transitions *at a given* $h\nu$. With our choice of parameters, this is equivalent to vary the effective-mass values m_6, m_{8h}, and m_7. For the Γ_8 bands (see Sec. 2 b of the Appendix), we find an energy change of the order of

$$\delta\varepsilon_{8h\text{-}6} \approx k\mathcal{P}(k\mathcal{P}/P^2)^2(m_0/m_{8h})(m_0/m^*)(\delta m^*/m^*) , \quad (5)$$

where m^* is one of the effective masses modified by δm^*. These changes, of the order of a small fraction of the energy in the Γ_{8h} band, can be neglected with respect to our energy resolution. In the case of the $\Gamma_7\rightarrow\Gamma_6$ transition, we obtain the energy variation (see Sec. 3 b of the Appendix):

$$\delta\varepsilon_{7\text{-}6} \approx -(k\mathcal{P}/2)(k\mathcal{P}/P^2)m_0(\delta m_6 m_6^{-2}-3\delta m_7 m_7^{-2}+2\delta m_{8h} m_{8h}^{-2}) . \quad (6)$$

The values of m_6 and m_{8h} are so precisely known that the dominant contribution in Eq. (6) originates from the uncertainty on the value of m_7. Then, if we fit m_7 to describe the variation of $\varepsilon_{7\text{-}6}$ vs $h\nu$, the uncertainty on m_7 is mostly related to our energy resolution $\delta\varepsilon$ through the formula

$$\delta m_7/m_7 \approx \tfrac{2}{3}(P^2/k\mathcal{P})(m_7/m_0)(\delta\varepsilon/k\mathcal{P}) . \quad (7)$$

Because in the present experiment $k\mathcal{P}$ is in the eV range, our determination of m_7 is accurate ($\delta m_7/m_7$ is of the order of a few percent). So we obtain $m_7=(0.19\pm0.01)m_0$, a value somewhat smaller than the approximate value $m_7=(0.21\pm0.02)m_0$ deduced from wavelength-modulated photovoltaic measurements.[9] The value of the uncertainty on our determination of m_7 results from a complete numerical treatment which takes into account the energy resolution and also the error bars of all the parameters used in the fit of the data. As in the framework of the Kane model the effective masses are not independent [see Eq. (A2)], we deduce $m_{8l}=(0.106\pm0.008)m_0$, in agreement with the value $m_{8l}=(0.12\pm0.01)m_0$ quoted in Ref. 12 within the error bars [the error δm_{8l} on our estimation of m_{8l} is mostly related to the error δm_7 on m_7 through the relation $\delta m_{8l}\approx 2\delta m_7(m_{8l}/m_7)^2$].

Finally, from the *numerical* calculation of the band dispersion in the Kane model, we obtain the fit of the experimental data plotted in Fig. 3 (full lines) which is very good even *at large excitation energy.*

V. CONCLUSION

The InP band-structure study, although very similar to the GaAs one in principle, appears to be technically much more difficult. Probably for this reason, previous attempts to apply the near-band-gap photoemission method to InP did not yield complete satisfactory results.[14] In the present work, the improvements in the measurement technique, as well as in the surface preparation, have proven to be decisive. Then we are able to measure accurately the energy positions of the subsidiary conduction valleys L_6, X_6, and X_{7c}, providing useful data for device modeling and pertinent values for pseudopotential calculations. Also in contrast to the GaAs case, it is possible to follow the promotion energy from the Γ_7 band throughout a wide photon-energy range. Because in the fit of the photoemission structure diagram, the only adjustable parameter is the spin-orbit-split band mass, we estimate it more directly than in other experiments. This precise determination is possible because we accurately measure *large* kinetic energies: the relative precision on our energy measurement is of the same order as in luminescence experiments which achieve meV resolution.[15]

ACKNOWLEDGMENTS

We are particularly indebted to G. Lampel for many fruitful discussions. We are grateful to R. Coquillé for providing us with InP substrates and to A. Ougazzaden for the MOCVD growth. We thank C. Hermann and Y. Lassailly for a critical reading of the manuscript. This work has been performed under Contract No. 87-224 with the Direction des Recherches, Etudes et Techniques (D.R.E.T.) de la Délégation Générale pour l'Armement. H.-J.D. is a member of D.R.E.T. Laboratoire de Physique de la Matière Condensée is "Unité de Recherche Associée D-1254 au Centre National de la Recherche Scientifique."

APPENDIX: ANALYTICAL STUDY OF THE STRUCTURE DIAGRAM

The following analysis is based on the $\mathbf{k}\cdot\mathbf{p}$ Kane model.[2] In this model, the $\mathbf{k}\cdot\mathbf{p}$ perturbation and the spin-orbit interaction are exactly diagonalized in the quasidegenerate band subset formed by the Γ_6, Γ_{8h}, Γ_{8l}, and Γ_7 bands. The expressions of the wave functions involve real coefficients a_i, b_i, and c_i, where the index i refers to the bands Γ_6, Γ_{8l}, and Γ_7, whereas the Γ_{8h} band remains uncoupled. Then, the remote-band interaction is added as a perturbation through matrix elements $\mathcal{A}$, $\mathcal{B}$, $\mathcal{C}$, $\mathcal{D}$, $\mathcal{F}$, and $\mathcal{G}$. These coefficients and matrix elements are all defined in Ref. 2.

The remote-band interaction introduces anisotropy in the electronic structure as warping and spin splitting of the bands. Nevertheless, in the Γ_{8h} band, the warping is only a small fraction of the energy in this band (the heavy-hole effective mass changes at most by 7% in InP between [100] and [111] directions)[12] and it only differs by the factor $b_i^2-2c_i^2$ in the other bands. The spin splitting is also small as it depends on the product $a_i b_i \mathcal{G}$ (see Sec. 1 of this appendix and Ref. 11) and is equal to zero along the [100] and [111] directions. It is thus readily checked that the effects of anisotropy are actually negligible with respect to our experimental energy resolution. Then, we calculate the band dispersion along the [100] direction. Adding the energy terms resulting from the remote-band coupling and the free-electron contribution to the solutions ε_i' and ε_{8h}' of the Kane secular equation, the expressions of the energy in the Γ_i and Γ_{8h} bands are

$$\varepsilon_i=\varepsilon_i'+\hbar^2k^2/2m_0+[a_i^2\mathcal{F}+b_i^2(\mathcal{C}+\mathcal{D})+c_i^2(\mathcal{A}+\mathcal{B})]k^2 , \tag{A1}$$

$$\varepsilon_{8h}=\hbar^2k^2/2m_0+(\mathcal{C}+\mathcal{D})k^2 ,$$

the energy origin being taken at the top of the valence band.

For small k values, these solutions describe four parabolic bands, the effective masses of which, m_6, m_{8h}, m_{8l}, and m_7 can be readily obtained. Conversely, the relevant combinations of Kane matrix elements can be simply expressed as a function of these masses. It also comes out from Eqs. (A1) that the valence effective masses are not independent one on the others but verify the relation:

$$m_0(m_{8l}^{-1}+m_{8h}^{-1}-2m_7^{-1})=2P^2\Delta/[3E_G(E_G+\Delta)] . \tag{A2}$$

Thus, as discussed in Sec. IV B of the main text, besides E_G, Δ, and P^2, we choose m_6, m_{8h}, and m_7 as the input parameters of the model [and estimate m_{8l} from Eq. (A2)]. The expressions of the matrix elements as a function of these parameters are

$$\begin{aligned} F&=(m_0/m_6)-(m_0/\mathcal{m}_6) ,\\ A+B&=2[(m_0/m_{8h})-(m_0/\mathcal{m}_{8h})]\\ &\quad -3[(m_0/m_7)-(m_0/\mathcal{m}_7)] ,\\ C+D&=(m_0/\mathcal{m}_{8h})-(m_0/m_{8h}) , \end{aligned} \tag{A3}$$

where A, B, C, D, and F are dimensionless quantities related to $\mathcal{A}$, $\mathcal{B}$, $\mathcal{C}$, $\mathcal{D}$, and $\mathcal{F}$ through relations of the type $A=(2m_0/\hbar^2)\mathcal{A}$. In these expressions, $\mathcal{m}_6$, $\mathcal{m}_{8h}$, and $\mathcal{m}_7$ are the effective masses calculated when the remote-band interaction is not taken into account (see Sec. II in Ref. 3).

Remark that, since F, $A+B$, and $C+D$ are differences between inverses of effective masses in m_0 units calculated with and without taking into account the remote-band interaction, these quantities must generally be of the order of unity. In the case of InP, the $\mathcal{m}_7$ and $\mathcal{m}_6$ values agree with the experimental determinations of m_7 and m_6 within about 25%; in contrast, the value $m_{8h}=0.56m_0$ is determined by the remote-band interaction, while $\mathcal{m}_{8h}=-m_0$. Then, the numerical values of the matrix elements are $F\approx-2.3$, $A+B\approx0.46$, and $C+D\approx-2.79$.

1. Approximate expressions of the band dispersion

In order to check the sensitivity of our experiments to the different parameters involved in the model, we use a

convenient analytical treatment of the Kane model developed in Ref. 3, Secs. III B 1 and III C. In this framework, simple approximate solutions of the Kane cubic equation for the Γ_6, Γ_7, and Γ_{8l} bands are derived which are very precise in the case of InP and in our photon energy range because $\Delta/E_G \ll 1$ and $E_G\Delta/(k\mathcal{P})^2 \ll 1$:

$$\begin{aligned}
&\varepsilon'_6=[(E_G-\Delta/3)/2]+\mathcal{E}_1 ,\\
&\varepsilon'_7=[(E_G-\Delta/3)/2]-\mathcal{E}_1 ,\\
&\varepsilon'_{8l}=-2\Delta/3 ,
\end{aligned} \tag{A4}$$

where

$$\mathcal{E}_1=\{(k\mathcal{P})^2+[(E_G+\Delta/3)/2]^2\}^{1/2} .$$

The corresponding approximations of the coefficients a_i^2, b_i^2, and c_i^2 are

$$\begin{aligned}
&a_6^2\approx c_7^2\approx \tfrac{1}{2}[1+(E_G+\Delta/3)/2\mathcal{E}_1] ,\\
&c_6^2\approx a_7^2\approx \tfrac{1}{2}[1-(E_G+\Delta/3)/2\mathcal{E}_1] ,\\
&b_6^2\approx b_7^2\approx 0 ,\\
&a_{8l}\approx c_{8l}^2\approx 0 ,\\
&b_{8l}^2\approx 1 .
\end{aligned} \tag{A5}$$

Then, the resulting description of the band dispersion which includes the remote-band interaction and the free electron contribution is given by

$$\begin{aligned}
\varepsilon_6=&[(E_G-\Delta/3)/2]+[(k\mathcal{P})^2/P^2][1+(F+A+B)/2]\\
&+[(k\mathcal{P})^2/\mathcal{E}_1][1+(E_G+\Delta/3)(F-A-B)/4P^2)]+[(E_G+\Delta/3)/2]^2/\mathcal{E}_1 ,\\
\varepsilon_{8h}=&-(m_0/m_{8h})(k\mathcal{P})^2/P^2 ,\\
\varepsilon_{8l}=&-2\Delta/3-(m_0/m_{8h})(k\mathcal{P})^2/P^2 ,\\
\varepsilon_7=&[(E_G-\Delta/3)/2]+[(k\mathcal{P})^2/P^2][1+(F+A+B)/2]\\
&-[(k\mathcal{P})^2/\mathcal{E}_1][1+(E_G+\Delta/3)(F-A-B)/4P^2)]-[(E_G+\Delta/3)/2]^2/\mathcal{E}_1 .
\end{aligned} \tag{A6}$$

We have numerically compared, in the case of InP, these expressions to the exact solutions of the Kane model and found that they are extremely accurate in the whole k range probed by the photon energies we used.

We now consider the influence of P^2 and of the effective masses m_6, m_{8h}, and m_7 on the photoemission structure diagram. We show this way that our results allow us to deduce an accurate value of m_7. We relate the uncertainty on this determination to the energy resolution. For that purpose, we calculate the variation of the promotion energy into the Γ_6 band of electrons excited from one of the Γ_{8l}, Γ_{8h}, or Γ_7 bands by optical absorption *at a given excitation energy* $h\nu$, when varying P^2, m_6, m_{8h}, or m_7. We denote the promotion energies from the Γ_{8l}, Γ_{8h}, and Γ_7 bands respectively as $\varepsilon_{8l\text{-}6}$, $\varepsilon_{8h\text{-}6}$, and $\varepsilon_{7\text{-}6}$. We will differentiate Eqs. (A6) with respect to these different parameters and use the relations

$$\varepsilon_{8l\text{-}6}-\varepsilon_{8l}=h\nu,\quad \varepsilon_{8h\text{-}6}-\varepsilon_{8h}=h\nu,\quad \varepsilon_{7\text{-}6}-\varepsilon_7=h\nu , \tag{A7}$$

where ε_{8l}, ε_{8h}, and ε_7 are the electron energies in the initial states. The results for the Γ_{8l} band are in fact not specifically reported here as they are analogous to those obtained for the Γ_{8h} band [the expressions of ε_{8l} and ε_{8h} given by Eqs. (A6) only differ by the constant term $-2\Delta/3$].

2. The $\Gamma_8 \rightarrow \Gamma_6$ transitions

a. Dependence on P^2

The promotion energy and $k\mathcal{P}$ changes when varying P^2 by δP^2 are

$$\delta\varepsilon_{8h\text{-}6}=(m_0/m_{8h})(k\mathcal{P}/P^2)[(k\mathcal{P}/P^2)\delta P^2-2\delta(k\mathcal{P})] \tag{A8}$$

and

$$\delta(k\mathcal{P})=(k\mathcal{P}/P^2)(\delta P^2/P^2)[\beta(E_G+\Delta/3)/4+(\alpha/2+m_0/m_{8h})\mathcal{E}_1]/d ;$$

where

$$\begin{aligned}
&\alpha=m_0(m_6^{-1}-3m_7^{-1}+2m_{8h}^{-1})=1+(F+A+B)/2+2P^2\Delta/3E_G(E_G+\Delta) ,\\
&\beta=m_0(m_6^{-1}+3m_7^{-1}-2m_{8h}^{-1})=(F-A-B)+2P^2(E_G+\Delta/3)/E_G(E_G+\Delta) ,\\
&d=1+[2+F+A+B+2(m_0/m_{8h})]\mathcal{E}_1/P^2+[(E_G+\Delta/3)(F-A-B)/4P^2][1+(E_G+\Delta/3)^2/4\mathcal{E}_1^2] .
\end{aligned}$$

Note that, because F and $A+B$ are of the order of unity, α is also of the order of unity while β is of the order of $2P^2/E_G$, i.e., much larger than unity. As the terms of the order of $k\mathcal{P}/P^2$ are negligible with respect to unity, d may be reasonably approximated to 1. So we get

$$\delta\varepsilon_{8h\text{-}6}\approx(m_0/m_{8h})[(k\mathcal{P})^2/P^2](\delta P^2/P^2)v \ , \tag{A9}$$

where

$$v=(\Delta/3E_G)[(E_G-\Delta/3)/(E_G+\Delta)]-(F-A-B)[(E_G+\Delta/3)/2P^2]$$
$$-(\mathcal{E}_1/P^2)\{2+F+A+B+(\Delta/3E_G)[2P^2/(E_G+\Delta)]+2(m_0/m_{8h})\} \ .$$

It can be readily checked that $|v|$ is smaller than unity. Then, the absolute value of the error on the promotion energy can be over-estimated by

$$\delta\varepsilon_{8h\text{-}6}\approx\varepsilon_{8h}(\delta P^2/P^2) \ . \tag{A10}$$

b. Dependence on the effective masses

Following the same procedure, we now consider the promotion-energy change when varying independently the values of the effective masses m_6, m_{8h}, and m_7, respectively, by δm_6, δm_{8h}, and δm_7. Then,

$$\delta\varepsilon_{8h\text{-}6}=(m_0/m_{8h})(k\mathcal{P}/P^2)[k\mathcal{P}(\delta m_{8h}/m_{8h})-2\delta(k\mathcal{P})]$$

and

$$\delta(k\mathcal{P})=k\mathcal{P}(\mathcal{E}_1/P^2)(1/d)[(m_0/m_6)(\delta m_6/m_6)a_6^2-3(m_0/m_7)(\delta m_7/m_7)c_6^2+(m_0/m_{8h})(\delta m_{8h}/m_{8h})(1+2c_6^2)] \ . \tag{A11}$$

With $d\approx1$, we get

$$\delta\varepsilon_{8h\text{-}6}\approx-2(m_0/m_{8h})[(k\mathcal{P})^2/P^2](\mathcal{E}_1/P^2)\{(m_0/m_6)(\delta m_6/m_6)a_6^2-3(m_0/m_7)(\delta m_7/m_7)c_6^2$$
$$+(m_0/m_{8h})(\delta m_{8h}/m_{8h})[1+2c_6^2-(m_{8h}/m_0)(P^2/2\mathcal{E}_1)]\} \ . \tag{A12}$$

Consequently, varying one of the effective masses m^* by δm^*, leads to a change in the final-state energy of the order of

$$\delta\varepsilon_{8h\text{-}6}\approx\varepsilon_{8h}(\mathcal{E}_1/P^2)(m_0/m^*)(\delta m^*/m^*) \ . \tag{A13}$$

c. Direct estimation of the spin-orbit energy

In the structure diagram, the plots of $\varepsilon_{8h\text{-}6}$ and $\varepsilon_{8l\text{-}6}$ lie on parallel lines distant of about 60 meV. In the case of these transitions we write the equations

$$\varepsilon_{8h\text{-}6}+(m_0/m_{8h})[(k_{8h}\mathcal{P})^2/P^2]=h\nu \ , \tag{A14}$$

$$\varepsilon_{8l\text{-}6}+(m_0/m_{8h})[(k_{8l}\mathcal{P})^2/P^2]+2\Delta/3=h\nu \ , \tag{A15}$$

where k_{8h} and k_{8l} are the respective values of the wave vector which correspond to the optical transitions from the Γ_{8h} or Γ_{8l} bands to the Γ_6 band. Therefore, we can identify the energy spacing $\varepsilon_{8h\text{-}6}-\varepsilon_{8l\text{-}6}$ to the change $\delta\varepsilon_{8h\text{-}6}$ in $\varepsilon_{8h\text{-}6}$ when varying $h\nu$ by $2\Delta/3$. Then, from Eq. (A14) we obtain

$$\delta\varepsilon_{8h\text{-}6}=\delta(h\nu)-(m_0/m_{8h})[2k\mathcal{P}\delta(k\mathcal{P})/P^2] \tag{A16}$$

and differentiating the first of Eqs. (A6), we deduce

$$2k\mathcal{P}\delta(k\mathcal{P})=\delta\varepsilon_{8h\text{-}6}/w \ , \tag{A17}$$

where

$$w=(2+F+A+B)/2P^2+\{1+[2-(k\mathcal{P}/\mathcal{E}_1)^2](F-A-B)(E_G+\Delta/3)/4P^2\}/2\mathcal{E}_1 \ .$$

The dominant term in w is $1/2\mathcal{E}_1$ so that

$$\varepsilon_{8h\text{-}6}-\varepsilon_{8l\text{-}6}=(2\Delta/3)/[1+(m_0/m_{8h})2\mathcal{E}_1/P^2] \ . \tag{A18}$$

To estimate $\mathcal{E}_1$, we neglect the correction due to the remote-band interaction and the free-electron contribution in the first of Eqs. (A6), i.e., we use $\varepsilon_6\approx\varepsilon_6'$, and obtain

$$\mathcal{E}_1=\varepsilon_{8h\text{-}6}-[(E_G-\Delta/3)/2]\ . \tag{A19}$$

Therefore, we have an expression which yields a direct estimate of Δ from the structure diagram

$$\Delta=\tfrac{3}{2}(\varepsilon_{8h\text{-}6}-\varepsilon_{8l\text{-}6})[1+(m_0/m_{8h})(2\varepsilon_{8h\text{-}6}-E_G+\Delta/3)/P^2]\ . \tag{A20}$$

We obtain $\Delta=0.114\pm0.030$ eV, in agreement with the value $\Delta=0.108\pm0.003$ eV reported in Ref. 9.

3. The $\Gamma_7\rightarrow\Gamma_6$ transition

a. Dependence on P^2

Combining the first and last of Eq. (A6), we remark that

$$\varepsilon_6=[(k\mathcal{P})^2/P^2][1+(F+A+B)/2]+(\varepsilon_6-\varepsilon_7)/2+(E_G-\Delta/3)/2\ . \tag{A21}$$

Then, similarly to Sec. 2 a of this Appendix, we obtain

$$\delta\varepsilon_{7\text{-}6}=(k\mathcal{P}/P^2)\{(2+F+A+B)\delta(k\mathcal{P})-[(k\mathcal{P})^2/P^2](\delta P^2/P^2)(\alpha/2)\} \tag{A22}$$

and

$$\delta(k\mathcal{P})=k\mathcal{P}\beta[(E_G+\Delta/3)/4P^2](\delta P^2/P^2)\{1+[(F-A-B)(E_G+\Delta/3)/4P^2][1+(E_G+\Delta/3)^2/4\mathcal{E}_1^2]\}^{-1}\ .$$

Here again the denominator of $\delta(k\mathcal{P})$ is nearly equal to 1. Then, replacing α and β by their expressions, we get

$$\begin{aligned}\delta\varepsilon_{7\text{-}6}=-[(k\mathcal{P})^2/P^2](\delta P^2/P^2)\{&(\Delta/3E_G)[P^2/(E_G+\Delta)]\\&-(2+F+A+B)[(F-A-B)(E_G+\Delta/3)/4P^2-(\Delta/6E_G)(E_G-\Delta/3)/(E_G+\Delta)]\}\ .\end{aligned} \tag{A23}$$

The term proportional to $(\Delta/3E_G)[P^2/(E_G+\Delta)]$ largely dominates. Then, within a good approximation

$$\delta\varepsilon_{7\text{-}6}=-k\mathcal{P}[k\mathcal{P}/(E_G+\Delta)](\Delta/3E_G)(\delta P^2/P^2)\ . \tag{A24}$$

b. Dependence on the effective masses

Analogously we have

$$\begin{aligned}\delta\varepsilon_{7\text{-}6}=(k\mathcal{P}/P^2)\{&(2+F+A+B)\delta(k\mathcal{P})-(k\mathcal{P}/2)[(m_0/m_6)(\delta m_6/m_6)-3(m_0/m_7)(\delta m_7/m_7)\\&+2(m_0/m_{8h})(\delta m_{8h}/m_{8h})]\}\end{aligned} \tag{A25}$$

and

$$\begin{aligned}\delta(k\mathcal{P})=k\mathcal{P}&[(E_G+\Delta/3)/4P^2][(m_0/m_6)(\delta m_6/m_6)+3(m_0/m_7)(\delta m_7/m_7)-2(m_0/m_{8h})(\delta m_{8h}/m_{8h})]\\&\times\{1+[(F-A-B)(E_G+\Delta/3)/4P^2][1+(E_G+\Delta/3)^2/4\mathcal{E}_1^2]\}^{-1}\ .\end{aligned}$$

We combine Eqs. (A25) and use the fact that the denominator of $\delta(k\mathcal{P})$ is nearly equal to 1; we obtain

$$\begin{aligned}\delta\varepsilon_{7\text{-}6}=-(k\mathcal{P}/2)(k\mathcal{P}/P^2)\{&(m_0/m_6)(\delta m_6/m_6)[1-(2+F+A+B)(E_G+\Delta/3)/2P^2]\\&-3(m_0/m_7)(\delta m_7/m_7)[1+(2+F+A+B)(E_G+\Delta/3)/2P^2]\\&+2(m_0/m_{8h})(\delta m_{8h}/m_{8h})[1+(2+F+A+B)(E_G+\Delta/3)/2P^2]\}\ .\end{aligned} \tag{A26}$$

Because $(2+F+A+B)(E_G+\Delta/3)/2P^2\ll1$, Eq. (A26) simply becomes

$$\delta\varepsilon_{7\text{-}6}=-(k\mathcal{P}/2)(k\mathcal{P}/P^2)[(m_0/m_6)(\delta m_6/m_6)-3(m_0/m_7)(\delta m_7/m_7)+2(m_0/m_{8h})(\delta m_{8h}/m_{8h})]\ . \tag{A27}$$

---

[1]H.-J. Drouhin, C. Hermann, and G. Lampel, Phys. Rev. B **31**, 3859 (1985).

[2]E. O. Kane, J. Phys. Chem. Solids **1**, 249 (1957).

[3]H.-J. Drouhin and J. Peretti, Phys. Rev. B, preceding paper, Phys. Rev. B **44**, 7993 (1991).

[4]H.-J. Drouhin and M. Eminyan, Rev. Sci. Instrum. **57**, 1052 (1986).

[5]H.-J. Drouhin, D. Paget, and J. Peretti, in *Proceedings of the Tenth European Conference on Surface Science, Bologna 1988,* edited by C. M. Bertoni, F. Manghi, and U. Valbusa [Surf.

Sci. **211/212**, 593 (1989)].
[6]J. Peretti, H.-J. Drouhin, and D. Paget, Phys. Rev. Lett. **64**, 1682 (1990).
[7]G. D. Pitt, Solid State Commun. **8**, 1119 (1970).
[8]W. J. Turner, W. E. Reese, and G. D. Pettit, Phys. Rev. **136**, A1467 (1964).
[9]P. Rochon and E. Fortin, Phys. Rev. B **12**, 5803 (1975).
[10]C. Hermann and C. Weisbuch, Phys. Rev. B **15**, 823 (1977).
[11]H. Riechert, H.-J. Drouhin, and C. Hermann, Phys. Rev. B **38**, 4136 (1988).
[12]J. Leotin, R. Barbaste, S. Askenazy, M. S. Skolnick, R. A. Stradling, and J. Tuchendler, Solid State Commun. **15**, 693 (1974).
[13]M. Helm, W. Knap, W. Seidenbusch, R. Lassnig, E. Gornik, R. Triboulet, and L. L. Taylor, Solid State Commun. **53**, 547 (1985).
[14]L. W. James, J. P. Van Dyke, F. Herman, and D. M. Chang, Phys. Rev. B **1**, 3998 (1970).
[15]G. Fasol, W. Ackenberg, H. P. Hughes, K. Ploog, E. Bauser, and H. Kano, Phys. Rev. B **41**, 1461 (1990).